Multistage VIPA etalons for high-extinction parallel Brillouin spectroscopy

Giuliano Scarcelli and Seok Hyun Yun

Harvard Medical School and Wellman Center for Photomedicine, Massachusetts General Hospital,
65 Landsdowne St., UP-522, Cambridge, Massachusetts 02139, USA
syun@hms.harvard.edu

Abstract: We demonstrate a high-resolution high-extinction parallel spectrometer for Brillouin spectroscopy of turbid samples. Cascading multiple VIPA etalons in the cross-axis configuration allowed us to achieve a high extinction ratio of up to 80 dB with sub-GHz resolution. Using a three-stage VIPA, we obtained the Brillouin spectra from Intralipid solutions at concentrations up to 10%.

References and links

1. B. Culshaw, C. Michie, P. Gardiner, and A. McGown, "Smart structures and applications in civil engineering," Proc. IEEE **84**(1), 78–86 (1996).
2. K. J. Koski, and J. L. Yarger, "Brillouin imaging," Appl. Phys. Lett. **87**(6), 061903 (2005).
3. E. W. Eloranta, "High spectral resolution Lidar in "Lidar: range-resolved optical remote sensing of the atmosphere"," in *Springer Series in Optical Sciences*, K. Weitkamp, ed. (Springer-Verlag, New York, 2005).
4. H. S. Lim, M. H. Kuok, S. C. Ng, and Z. K. Wang, "Brillouin observation of bulk and confined acoustic waves in silica microspheres," Appl. Phys. Lett. **84**(21), 4182–4184 (2004).
5. G. Scarcelli, and S. H. Yun, "Confocal Brillouin microscopy for three-dimensional mechanical imaging," Nat. Photonics **2**(1), 39–43 (2007).
6. T. Still, R. Sainidou, M. Retsch, U. Jonas, P. Spahn, G. P. Hellmann, and G. Fytas, "The "music" of core-shell spheres and hollow capsules: influence of the architecture on the mechanical properties at the nanoscale," Nano Lett. **8**(10), 3194–3199 (2008).
7. P. Benassi, R. Eramo, A. Giugni, M. Nardone, and M. Sampoli, "A spectrometer for high-resolution and high-contrast Brillouin spectroscopy in the ultraviolet," Rev. Sci. Instrum. **76**(1), 013904 (2005).
8. T. Matsuoka, K. Sakai, and K. Takagi, "Hyper-resolution Brillouin–Rayleigh spectroscopy with an optical beating technique," Rev. Sci. Instrum. **64**(8), 2136–2139 (1993).
9. J. R. Sandercock, "Some recent developments in Brillouin scattering," RCA Rev. **36**, 89–107 (1975).
10. G. Scarcelli, P. Kim, and S. H. Yun, "Cross-axis cascading of spectral dispersion," Opt. Lett. **33**(24), 2979–2981 (2008).
11. P. Jacquinot, "The luminosity of spectrometers with prisms gratings or Fabry-Perot etalons," J. Opt. Soc. Am. **44**(10), 761–765 (1954).
12. H. Z. Cummins, and R. W. Gammon, "Rayleigh and Brillouin scattering in liquids – Landau–Placzek ratio," J. Chem. Phys. **44**, 2785–2796 (1966).
13. A. Vega, A. M. Weiner, and C. Lin, "Generalized grating equation for virtually-imaged phased-array spectral dispersers," Appl. Opt. **42**(20), 4152–4155 (2003).
14. S. J. Xiao, A. M. Weiner, and C. Lin, "A dispersion law for virtually imaged phased-array spectral dispersers based on paraxial wave theory," IEEE J. Quantum Electron. **40**(4), 420–426 (2004).
15. K. J. Koski, J. Muller, H. D. Hochheimer, and J. L. Yarger, "High pressure angle-dispersive Brillouin spectroscopy: A technique for determining acoustic velocities and attenuations in liquids and solids," Rev. Sci. Instrum. **73**(3), 1235–1241 (2002).
16. E. Duval, A. Boukenter, and B. Champagnon, "Vibration eigenmodes and size of microcrystallites in glass: Observation by very-low-frequency Raman scattering," Phys. Rev. Lett. **56**(19), 2052–2055 (1986).
17. L. M. Zhang, S. F. Yu, M. C. Nowell, D. D. Marcenac, J. E. Carroll, and R. G. S. Plumb, "Dynamic analysis of radiation and side-mode suppression in a second-order DFB laser using time-domain large-signal traveling wave model," IEEE J. Quantum Electron. **30**(6), 1389–1395 (1994).

1. Introduction

Brillouin scattering spectroscopy is a popular technique for material characterization [1–3]. The interaction between incident light and acoustic phonons in a sample is interrogated by the

spectral shift of the scattered light, providing information about the acoustic, thermodynamic and viscoelastic properties of material [4–6]. However, Brillouin scattering is a relatively weak process in the spontaneous regime, and the optical frequency shift is small, in the order of 10 GHz. In most situations, elastically scattered light due to Rayleigh scattering or optical reflections is orders-of-magnitude stronger than Brillouin signal. Therefore, a suitable Brillouin spectrometer should offer both sub-GHz spectral resolution and high spectral contrast (or extinction). Without sufficient suppression of elastically scattered light, the residual component of elastic scattering may overshadow or overlap with the dispersed spectrum, making it difficult to accurately measure the Brillouin spectrum.

Previously, the stringent requirement on spectral resolution and extinction had been met by scanning-grating monochromators [7], optical beating methods [8], and multiple-pass scanning Fabry-Perot interferometers [9]. In all these methods, each spectral component is measured sequentially. Consequently, acquisition of a single Brillouin spectrum typically required a few minutes to several hours, depending on the insertion loss of the instrument. The slow acquisition time limited Brillouin spectroscopy to point-sampling or static measurements.

Recently, we introduced a novel non-scanning Brillouin spectrometer employing a virtually-imaged phased array (VIPA) etalon. The ability to collect all spectral components simultaneously with low insertion loss enabled us to acquire Brillouin spectra within just a few seconds. However, the single VIPA etalon we used had an extinction of only about 30 dB and therefore only permitted measurements for nearly transparent samples.

We also recently developed a method of cascading multiple diffraction gratings in an orthogonal-axis configuration to improve the extinction [10]. The cross-axis cascade approach offers a simple way to separate and filter out the stray light from the spectral signal after each stage and thereby to reduce the background and crosstalk substantially. Here, we describe how we've applied the cross-axis cascading concept to VIPA etalons, demonstrating a two-stage and a three-stage VIPA spectrometer with an extinction ratio of 55 dB and 80 dB, respectively. Our results represent a crucial step towards the application of Brillouin scattering spectroscopy to turbid samples, such as biological tissues.

2. Background: Single-stage VIPA spectrometer

Figure 1(a) illustrates the schematic of our experimental setup for Brillouin spectroscopy. The laser light in a single longitudinal mode at 532 nm passes through a neutral density (ND) filter and a beam splitter, and is focused into the sample via an aspheric lens (f = 11 mm, NA = 0.3). The backward scattered light is collected by the same lens and coupled into a single-mode fiber by an objective lens (f = 6 mm, NA = 0.25). The optical fiber delivers the light into the VIPA spectrometer.

The VIPA etalon is conceptually similar to a tilted Fabry-Perot etalon [11]. It has three different coating areas. The front surface has a highly reflective (HR) coating (R1>99.9%), except for a narrow stripe with anti-reflection (AR) coating, through which the input optical beam is coupled. The back surface has a partially reflective coating (R2~90%). As shown in Fig. 1(b), the input beam is focused into the etalon by a cylindrical lens and enters the tilted (at an angle α) etalon. It is important to align the beam focus close to the boundary between the HR and AR regions to minimize the tilt angle (to maximize the finesse) while minimizing insertion loss. Inside the etalon, the beam undergoes multiple internal reflections and produces an array of output beams with increasing optical path (phase) delays. The interference among the phased array of beams provides large angular dispersion so that different frequency components are emitted at different angles, $\phi(\lambda)$. A spherical lens translates the angular separation into a spatial separation in the plane of a CCD camera.
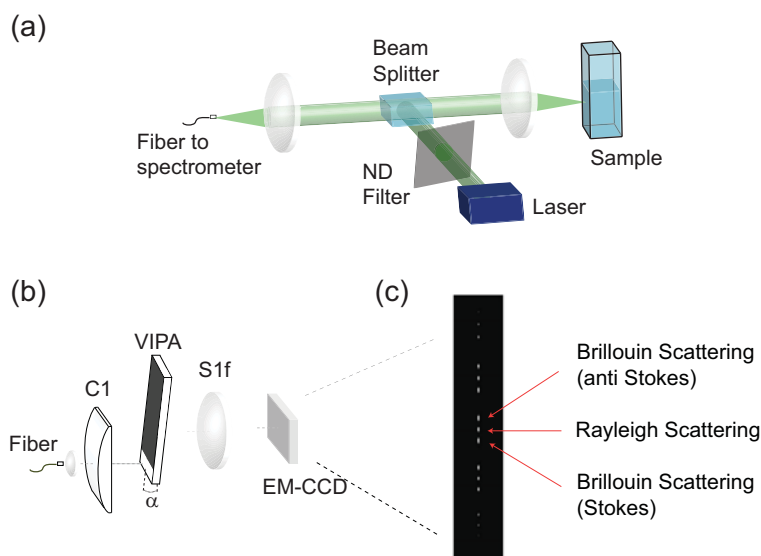
Fig. 1. (a) Confocal Brillouin spectroscopy setup used in all experiments. (b) Schematic of a single-stage VIPA spectrometer, consisting of a cylindrical lens (C_1), a VIPA etalon, a spherical lens (S_{1f}) and a CCD camera. (c) Brillouin spectrum obtained from Toluene sample (10 mW, 1 sec). The spectrum in each diffraction order of the etalon shows a triplet comprising Rayleigh, Brillouin Stokes and anti-Stokes peaks.

Figure 1(c) illustrates a typical single-frame record of the optical spectrum obtained from Toluene as sample. In each diffraction order, the spectrum comprises three peaks corresponding to Rayleigh scattering in the center and Stokes and anti-Stokes Brillouin scattering at both sides. The triplet pattern is replicated in different diffraction orders. The magnitude of Rayleigh scattering is comparable to those of Brillouin scattering. The ratio is known as Landau-Placzek ratio, which is typically close to one for transparent liquids [12]. However, the central peak can increase by several orders of magnitude for nontransparent turbid samples, such as Intralipid at high concentrations.

It is relatively easy to align the VIPA etalon with high throughput efficiency, because all the light coupled into the VIPA etalon is diffracted forward (like an echelle grating). This contrasts with a conventional Fabry-Perot etalons having HR coating on both surfaces, where interference patterns in both forward and backward directions are produced and any misalignment directly results in optical loss.

3. Principle of cross-axis cascading with VIPA etalons

Figure 2 illustrates the principle of cross-axis cascading with VIPA etalons to improve the extinction. In the first stage, Fig. 2(a), the VIPA is aligned along the vertical direction and the spectral pattern is dispersed vertically. When the sample is not transparent or when there are strong optical reflections, the elastic scattering component increases dramatically. If the ratio between elastic scattering (dark-green circles) and Brillouin scattering (light-green circles) exceeds the spectral extinction of the spectrometer, a crosstalk signal appears along the spectral axis (green line). This "stray light" can easily overwhelm the weak Brillouin signal.

In a double-VIPA spectrometer, Fig. 2(b), the second etalon is placed orthogonally to the first one. The spectral pattern exiting the first stage enters the second etalon through the input window. Both etalons disperse light, in orthogonal directions, so the overall spectral axis of the double-spectrometer lies along a diagonal direction, at 135° from the horizontal axis if the etalons have identical dispersive power. The second etalon will separate Brillouin signal from crosstalk because, although spatially overlapped after the first stage, their frequencies at each

spatial location are different. So, after the second stage, while the Brillouin spectrum lies on a diagonal axis, crosstalk components due to the limited extinctions of the etalons are separated and mostly confined to the horizontal and vertical axis.
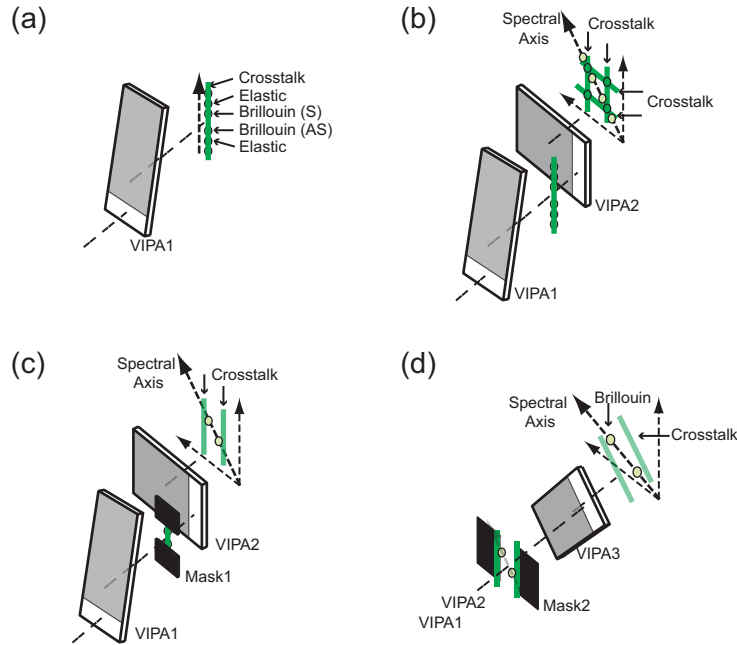

Fig. 2. Illustration of the principle of multiple VIPA cascading. (a) In a single stage, Brillouin signal and crosstalk overlap. (b) In a double spectrometer, the spectral axis is diagonal, while crosstalk is confined to horizontal and vertical directions. (c) A mask between first and second stages can filter out part of the crosstalk component. (d) A second mask between second and third etalon further reduces the crosstalk component.

Besides spatial separation of signal and stray light, the double stage spectrometer also allows selective spectral filtering, as shown in Fig. 2(c). An appropriate aperture mask can be placed at the focal plane of VIPA1, where a highly-resolved spectral pattern is formed. Unwanted spectral components are thus blocked and only the desired portion of the spectrum is allowed to pass to the second stage. For optimal performance, it is often desirable to maintain only two Brillouin peaks (Stokes and anti-Stokes from two adjacent orders) and have a vertical mask cut off all elastic scattering peaks. This greatly reduces crosstalk in VIPA2 and helps avoid saturation of the CCD camera by pixels hit by unfiltered elastic scattering peaks.

This strategy of cross-axis cascade can be extended to a third stage. In a triple-VIPA spectrometer (Fig. 2d), VIPA3 is placed perpendicular to the spectral axis of the preceding two stages, so that the Brillouin spectrum can enter through the input window. A second mask is employed to further reduce crosstalk after VIPA2. Due to the combined dispersion of the three etalons, the overall spectral axis is further rotated, at 170° if all the etalons have the same dispersive power.
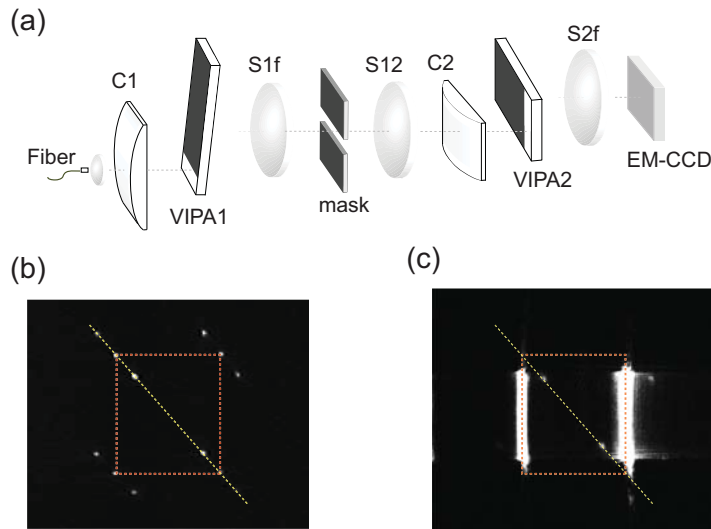
4. Two-stage VIPA spectrometer

Fig. 3. (a) Schematic of a two-stage VIPA spectrometer. In between stages a mask and a relay spherical lens are inserted. (b) Brillouin spectrum of methanol sample (10 mW, 1 sec), obtained with the spectrometer. For illustration purpose only, we drew a line (dashed, yellow) to indicate the spectral dispersion axis of the double-stage spectrometer and a square (dotted, orange) to show the vertical and horizontal axes. (c) Brillouin spectrum of a 0.01% Intralipid solution measured at 7 mW and integration time of 1 sec. The vertical mask cut off the stray light in the horizontal axis, but strong residues are seen as saturated vertical lines.

We implemented the cross-axis cascading principle to build a two-stage spectrometer. Figure 3(a) shows the schematic of the experimental setup. Input light is focused into the first etalon by a vertical cylindrical lens C_1 (f = 200 mm); after multiple reflections inside VIPA1 the beam passes through a relay telescope composed of spherical lens S_{1f} (f_1 = 200 mm), a spatial filter in the focal plane of S_{1f}, and spherical lens S_{12} (f_{12} = 200 mm). Light then enters the second stage through cylindrical lens C_2 (f = 200 mm), goes through the horizontally oriented VIPA2 and is focused by spherical lens S_{2f} (f_2 = 200 mm) onto the plane of the CCD camera (Cascade 650, Roper Scientific). In a simpler but equally effective design, S_{1f} can be replaced by a vertical cylindrical lens and C_2 is removed so that S_{12} serves both as collimator for the first stage relay telescope and as input lens for the VIPA2.

The propagation direction of the output beam after a VIPA etalon is largely unchanged and remains in the horizontal plane. Therefore, there is no need of an image rotator, such as a Dove prism, as used in our previous cross-axis grating spectrometer [10].

Figure 3(b) shows a representative spectrum from methanol, as captured by the CCD camera. The triplet of Rayleigh-Brillouin scattering peaks are dispersed along a diagonal axis, and replicated in several diffraction orders arranged in a 2-dimensional pattern (four orders are seen here). The spectral dispersion axis (yellow dashed line) in the CCD plane is at about 135° with respect to the vertical/horizontal axis. Here, the sample is transparent so the elastic scattering component is comparable to Brillouin signal. In non-transparent samples, however, excess elastic scattering lies along the horizontal and vertical directions (orange dotted lines). This situation is clearly illustrated in Fig. 3(c), for the case of a 0.01% aqueous solution of Intralipid, where two Brillouin peaks (Stokes and anti-Stokes) from adjacent diffraction orders are seen, together with strong crosstalk signal that was separated from the Brillouin peaks in the second stage. The horizontal crosstalk component was blocked with the mask between the first and second stage, as illustrated in Fig. 2(c).

5. Three-stage VIPA spectrometer

A three-stage VIPA spectrometer can be constructed by adding a third VIPA as depicted in Fig. 4(a). We built the experimental setup using three identical VIPA etalons (R1 = 99.99% and R2 = 92%) oriented vertically (90°), horizontally (180°), and at 225°, respectively. After VIPA2, the beam passes through a relay telescope composed by two spherical lenses S_{2f} (f_2 = 200 mm) and S_{23} (f_{23} = 150mm) and a spatial filter in the focal plane of S_{2f}. The beam is focused into the diagonal VIPA3 by a cylindrical lens C_3 (f = 500 mm). The final pattern is formed by a spherical lens S_{3f} (f_3 = 150 mm) onto the CCD camera located in the focal plane of S_{3f}.

Figure 4(b) shows a representative Brillouin spectrum obtained from a 0.1% aqueous solution of Intralipid with the three-stage spectrometer. Two Stokes and anti-Stokes peaks in two adjacent diffraction orders are clearly seen and well separated from residual stray light ('Elastic' in Fig. 4(b)). We note that all other spectral signatures are blocked by the two masks after the first and second stages. By plotting pixel intensity along the spectral axis, the Brillouin spectrum of a sample can be quantified. Figure 4(c) shows an example of this measurement for Plexiglass. The spectrum was acquired with 21 mW laser power and 1 s acquisition time. Given the known Brillouin linewidth (~250 MHz) of Plexiglass, we used the experimental linewidth to compute the instrumental spectral linewidth of the three-stage interferometer. The estimated spectral resolution of our setup was about 700 MHz, which corresponds to a high finesse of about 40.
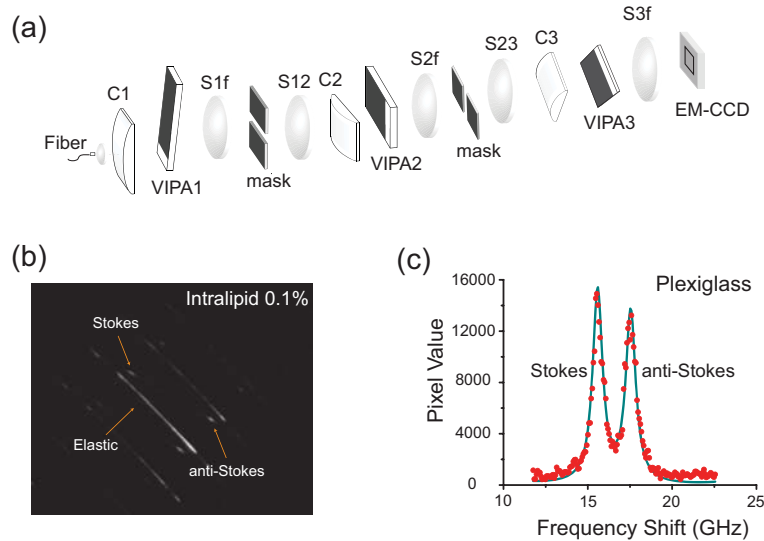

Fig. 4. (a) Experimental setup of a three-stage VIPA spectrometer. (b) Brillouin spectrum of an Intralipid solution (0.1%) sample (21 mW, 1 sec). Only Stokes and anti-Stokes peaks from adjacent diffraction orders are shown after filtering by the masks. (c) Brillouin spectrum of Plexiglass sample (21 mW, 1 sec).

In terms of optical throughput, 55% of incident light was transmitted through the first stage, 40% of which passed through the second stage, and the third stage had 30% throughput efficiency. Therefore, the overall throughput of the instrument was 7%. The typical throughput of a single-stage VIPA spectrometer ranges from 50% to 70%, where a higher loss results from a shallower tilt angle, yielding higher finesse. The additional losses in the second and third stages are largely attributed to the generation of multiple diffraction orders, because only one of them is coupled into the next stage. With further optimization of VIPA etalons and relay optics, the insertion loss of multi-stage etalons can be improved.

6. Extension to *N*-stages

Following the same cascading principle, a multiple VIPA interferometer of *N* stages can be built. Here, the *k*-th VIPA is oriented at an appropriate angle to accept the spectrum dispersed through the preceding *k*-1 stages. The building block of each stage is modular, comprised of a cylindrical lens C_k, an etalon $VIPA_k$, a spherical Fourier transform lens S_{kf} with focal length f_k, a mask and a spherical relay lens $S_{k,k+1}$ of focal length $f_{k,k+1}$.

Figure 5 illustrates how the orientations of the etalons and the spectral axes change in a multi-stage interferometer. In the first stage, the VIPA is oriented along the direction v1 at an angle θ_1 with respect to the horizontal axis ($\theta_1 = 90°$ in our experiment), and its spectral dispersion direction, d1, is parallel to v1 with $\psi_1 = \theta_1$. In the double-VIPA interferometer, the second etalon is aligned along v2 at an angle $\theta_2 = \psi_1 \pm \pi/2$, perpendicular to the spectral direction of the first stage d1 ($\theta_2 = 180°$ in our experiment). After the two etalons, the spectrum emerges at an angle ψ_2 ($\psi_2 = 135°$ in our experiment; see Fig. 3b) along spectral dispersion direction, d2. In a three-stage interferometer, the third VIPA must be oriented perpendicular to d2, at an angle $\theta_3 = \psi_2 \pm \pi/2$ ($\theta_3 = 225°$ in our experiment), which is depicted in Fig. 5(c). This arrangement results in a final dispersion direction s3 at an angle ψ_3.
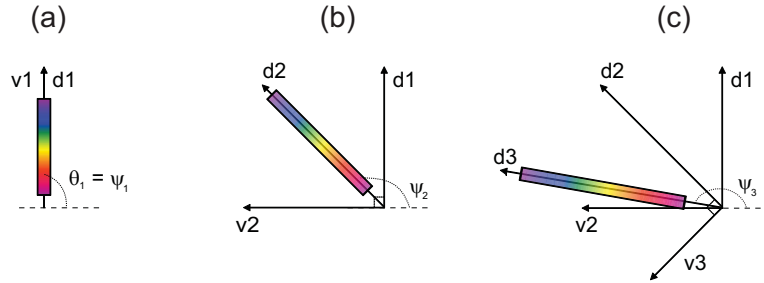
Fig. 5. Illustration of the relationship between the orientation of the VIPA etalon and dispersion axis at each stage. (a) In a single stage, the orientation of the VIPA etalon (v1) and spectral dispersion axis (d1) coincide. (b) In a two-stage spectrometer, the second etalon axis (v2) is perpendicular to d1, and the overall spectral dispersion is diagonal (d2). (c) In a three-stage spectrometer, the third etalon axis (v3) is perpendicular to the d2.

For each stage, the dispersion angle, ϕ_k, imposed on a beam of wavelength λ by the kth VIPA interferometer was previously derived in both plane-wave and paraxial approximations [13,14]. The focal length f_k of the spherical lens, S_{kf}, after the VIPA determines the linear dispersion power, s_k, of the kth stage:

$$s_k = \phi_k * f_k. \tag{1}$$

Since telescopes are used to link two subsequent VIPA stages, the overall linear dispersion also depends on the magnifications introduced by such optical systems. Namely, each kth stage introduces a magnification $M_k = f_k / f_{k-1}$ on the spectral pattern obtained by the previous *k*-1 stages, so that the effective linear dispersion, s'_k, due to the kth stage is given by:

$$s'_k = s_k * M_N * M_{N-1} * ... * M_{k+1}. \tag{2}$$

Therefore, along the overall spectral axis, the total linear dispersion, S_N, of an N-stage multiple VIPA interferometer is calculated to be:

$$S_N = \sqrt{\sum_1^N s'^2_k}, \tag{3}$$

which suggests a theoretical improvement in spectral resolution. When all the spectral dispersions are equal, i.e. $s'_1 = s'_2 = \ldots = s'_N \equiv s$, the total dispersion becomes $S_N = \sqrt{N} * s$.

Knowing the spectral dispersion and the optical magnification introduced by each stage, the overall dispersion axis can be computed. It can be shown:

$$\psi_{k+1} - \psi_k = \tan^{-1}(s'_{k+1}/S_k) \rightarrow \tan^{-1}(1/\sqrt{k}), \tag{4}$$

$$\theta_{k+1} - \theta_k = \tan^{-1}(s'_k/S_{k-1}) \rightarrow \tan^{-1}(1/\sqrt{k-1}), \tag{5}$$

where the expressions marked with arrows apply in the case equal dispersion and unit magnification for all stages.

In our experiments, we obtained spectral dispersion angles of, $\psi_1 = 90°$, $\psi_2 = 135°$ and $\psi_3 = 150°$. The third dispersion angle is smaller than 170°, the value that would have resulted if all the three stages had identical linear dispersion. In our case, the third stage actually had a lower linear dispersion with respect to the first and second stages because of the shorter focal length of S_{3f} and the slightly larger tilt angle of VIPA3. The tilt was necessary to accommodate the expanded beam after the second stage (~15 mm), which could be avoided by using a cylindrical lens C_3 with longer focal length or an additional telescope.

In terms of extinction, a single VIPA spectrometer has extinction, C proportional to its finesse squared: $C \approx 4F^2/\pi^2$, for an input beam with Airy profile [15]. After N VIPA etalons of equal finesse F, the spectral extinction or contrast improves, in principle, to:

$$C \approx (4F^2/\pi^2)^N. \tag{6}$$

We experimentally measured the improvement in extinction, as described in the next section.

7. Measurement of the extinction ratio

We compared the extinction performance of single-stage, two-stage and three-stage VIPA spectrometers by coupling the single mode laser light directly into the spectrometer and placing a CCD camera in the focal planes of S_{1f}, S_{2f}, and S_{3f}, respectively To overcome the limited dynamic range of the CCD, we recorded the spectrum at various optical power levels, with calibrated neutral density (ND) filters of optical densities in the range from 0 to 7. Subsequently, the full dynamic range spectrum was reconstructed by rescaling the recorded raw spectra according to the respective attenuation levels. The results are shown in Fig. 6. The two peaks at the relative frequencies of 0 and 33 GHz correspond to the stray laser line. The free spectral range (FSR) of 33 GHz is nearly the same as the FSR of the VIPA etalons in the spectrometer. The normalized signal, therefore, represents the crosstalk of the laser line due to finite extinction of the spectrometer. The single-stage VIPA shows an extinction level of about 30 dB over a wide frequency range between 5 and 25 GHz. The extinction is improved to 55 dB with two stages and to nearly 80 dB with three VIPA etalons in the middle of the frequency range. It might be possible to improve the extinction up to 90 dB by minimization of aberrations in the optical system and improvements of beam shape or profile.
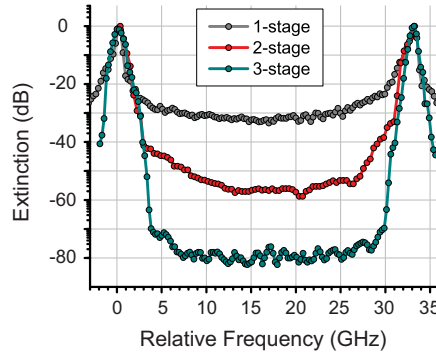
Fig. 6. Spectral response of a single- (gray), double- (red), and triple- (green) spectrometer to the single laser line at 532 nm. The normalized background signal shows improvement in spectral contrast from 30 dB (single-stage) to 55 dB (two-stage) and 80 dB (three-stage).

8. Brillouin measurement of Intralipid solutions

Finally, we applied the multi-stage spectrometer to parallel Brillouin spectroscopy of turbid samples, using aqueous solutions of Intralipid at various concentrations. Because of the low extinction of the single VIPA spectrometer, it was impossible to detect any Brillouin signal even at minimal concentrations (10^{-7}%) of Intralipid. Figure 7 shows the comparison between two-stage and three-stage spectrometers. For this measurement, we placed the Intralipid solution inside a plastic cuvette and adjusted the confocal microscope to focus light just inside the liquid sample. We used higher incident power (21 mW) in the three-stage measurement than the two-stage measurement (7 mW) in order to offset the excess loss induced by the third stage. The two sets of experiments used the same spectrum acquisition time of 1 s. The magnitudes of Brillouin signal and elastic crosstalk (background) were measured at different intralipid concentrations.
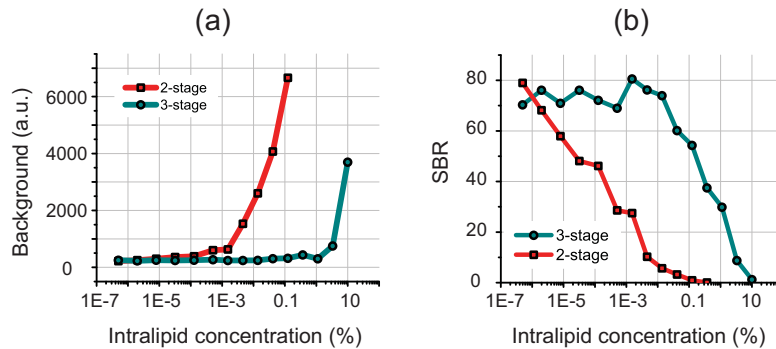

Fig. 7. (a) Background elastic scattering from Intralipid solution, measured by the two-stage (red) and three-stage (green) spectrometer at 7.5 GHz as a function of Intralipid concentration. (b) Brillouin signal to background ratio (SBR) as a function of Intralipid concentration for two-stage (red) vs three-stage (green) spectrometer.

The Brillouin frequency shift of the Intralipid solutions is close to 7.5 GHz, similar to that of pure water. In Fig. 7(a), we plot the amount of elastically-scattered light in the area around the Brillouin frequency of 7.5 GHz. It is noticeable that the two-stage spectrometer can effectively suppress the elastic background up to 0.001% Intralipid concentration. Beyond 0.001%, the background increases exponentially with concentration. In contrast, the three-stage spectrometer completely suppressed the background signal up to 5% Intralipid concentration. The effective suppression of the elastic-scattering component results in a much

higher signal-to-background ratio (SBR) of the Brillouin spectral measurement. In Fig. 7(b), we plot the measured SBR as a function of concentration. With the two-stage spectrometer, SBR rapidly degrades with increasing concentration and drops below one at 0.1% concentration. However, the three-stage spectrometer is able to measure the Brillouin spectrum up to 10% Intralipid concentration, clearly demonstrating the benefit of the third stage.

9. Conclusion

In conclusion, we have demonstrated multi-stage VIPA spectrometers featuring high spectral extinction, sub-GHz spectral resolution and parallel detection. The 80-dB extinction of the three-stage spectrometer enabled us to measure the Brillouin scattering spectrum of Intralipid solutions up to 10% concentration. Intralipid solutions at concentration between 1% and 10% have been widely used as tissue phantoms as the scattering properties are similar. Therefore, our experimental results indicate that three-stage VIPA interferometry may be suitable for high-speed parallel Brillouin spectroscopy in biological tissues. In addition to Brillouin spectroscopy, multi-stage VIPA spectrometers might find other applications such as the characterization of sub-micron particle aggregates via low-frequency Raman scattering spectroscopy [16] and of side-mode suppression ratio of laser sources [17].

Acknowledgements